Monitoring the development of xenograft triple-negative breast cancer models using diffusion-weighted magnetic resonance imaging

Renu M Stephen[1], Mark D Pagel[1,2,3], Kathy Brown[1], Amanda F Baker[1,4], Emmanuelle J Meuillet[1,5] and Robert J Gillies[6]

[1]Arizona Cancer Center, University of Arizona, Tucson, AZ 85724; [2]Department of Chemistry and Biochemistry; [3]Department of Biomedical Engineering, University of Arizona, Tucson, AZ 85721; [4]Hematology/Oncology Section, College of Medicine, University of Arizona, Tucson, AZ 85724; [5]Department of Nutritional Sciences, University of Arizona, Tucson, AZ 85721; [6]Department of Imaging, H Lee Moffitt Cancer Center and Research Institute, 12902 Magnolia Drive, Tampa, FL 33612, USA
Corresponding author: Robert J Gillies. Email: Robert.Gillies@moffitt.org

Abstract

Evaluations of tumor growth rates and molecular biomarkers are traditionally used to assess new mouse models of human breast cancers. This study investigated the utility of diffusion weighted (DW)-magnetic resonance imaging (MRI) for evaluating cellular proliferation of new tumor models of triple-negative breast cancer, which may augment traditional analysis methods. Eleven human breast cancer cell lines were used to develop xenograft tumors in severe combined immunodeficient mice, with two of these cell lines exhibiting sufficient growth to be serially passaged. DW-MRI was performed to measure the distributions of the apparent diffusion coefficient (ADC) in these two tumor xenograft models, which showed a correlation with tumor growth rates and doubling times during each passage. The distributions of the ADC values were also correlated with expression of Ki67, a biomarker of cell proliferation, and hypoxia inducible factor (HIF)-1α and vascular endothelial growth factor receptor-2 (VEGFR2), which are essential proteins involved in regulating aerobic glycolysis and angiogenesis that support tumor cell proliferation. Although phosphatase and tensin homolog (PTEN) levels were different between the two xenograft models, AKT levels did not differ nor did they correlate with tumor growth. This last result demonstrates the complexity of signaling protein pathways and the difficulty in interpreting the effects of protein expression on tumor cell proliferation. In contrast, DW-MRI may be a more direct assessment of tumor growth and cancer cell proliferation.

Keywords: magnetic resonance imaging, diffusion-weighted MRI, breast cancer, mouse model

Experimental Biology and Medicine 2012; **237**: 1273–1280. DOI: 10.1258/ebm.2012.011326

Introduction

Mouse models of breast cancer have become essential resources for studying cellular mechanisms of progression by extending *in vitro* studies to an *in vivo* context.[1,2] Mouse models have also been useful for studying the hallmarks of the *in vivo* tumor microenvironment, which cannot be recapitulated with *in vitro* studies.[3] Although many types of breast cancer cells have been obtained and characterized *in vitro*, only a small set of mouse models have been developed to study some cellular pathways and hallmarks of the tumor microenvironment.[4] Most of these mouse models have been selected for fast growth rates to facilitate the rapid development of consistent tumors in mice, which does not necessarily match the characteristics of slower-growing tumors in patients. Furthermore, cancer cell lines that have been extensively passaged in mice to ensure tumor growth may select for specific traits, and therefore may not reflect the heterogeneity of human breast cancer as well as low-passage cancer cell lines. For this reason, the National Cancer Institute has strongly emphasized the need to develop new mouse models that recapitulate other cellular mechanisms and hallmarks of the tumor microenvironment of human breast tumors.[5,6] Mouse models of triple-negative breast cancer are particularly needed due to the interest in developing new treatments for this category of breast cancer.

Tumor size is the primary method used to monitor the proliferation of new xenograft models; yet tumor size essentially reflects the growth of the tumor periphery, and is relatively insensitive to the cellular status of the tumor core that

may exhibit cell apoptosis, necrosis, lipid deposition or vasogenic edema.[7] Furthermore, monitoring tumor size only indirectly monitors the status of the tumor microenvironment, which is also critical for tumor proliferation. Perhaps most importantly, monitoring tumor size does not necessarily reflect cell density, which is an important biomarker for cell proliferation and tumor growth.

Tumor development in mice has also been monitored using immunohistochemical analysis of proliferation biomarkers, such as Ki67 that down-regulates apoptosis.[8,9] These biopsies can directly evaluate the status of signaling networks, characteristics of the tumor microenvironment and cell density. Yet, the limited frequency and limited spatial coverage of tissue biopsies can lead to sampling artifacts and limit the use of this method for assessing new tumor models. Therefore, a different method is needed that can assess the cellular proliferation of new tumor models by monitoring the tumor microenvironment at the meso (micron to millimeter) scale, can evaluate cell densities, and can non-invasively and longitudinally appraise entire volumes of tumor tissues in mouse models of human cancers.

Diffusion-weighted magnetic resonance imaging (DW-MRI) meets these criteria by non-invasively measuring the apparent diffusion coefficient (ADC) of water within *in vivo* tissues throughout an entire tissue volume.[10,11] This imaging method does not require exogenous contrast agents and therefore can be performed during longitudinal studies. The ADC is sensitive to biological barriers that reduce water diffusion at the meso scale, such as cell plasma membranes and intracellular organelles. ADC measurements can be used to compare tissues with different intracellular and extracellular compartments, and thus can evaluate relative differences in cell densities between tumors and normal tissues.[12–14] Many preclinical and clinical studies have established that ADC values increase in response to cytotoxic therapies that alter cell densities.[15–17] DW-MRI can also characterize regions of apoptosis or necrosis that cause changes in cell density within solid tumors.[18–21]

Despite the great utility of DW-MRI for many biomedical applications, the utility of DW-MRI for evaluating new tumor models has not yet been established. To investigate this utility, we developed xenograft mouse models of 11 new low-passage tumor cell lines from patients, and measured the ADC values of the two cell lines that showed good tumor growth during three passages in a mouse model. These DW-MRI results were compared with growth rates and doubling times of the tumors, and with protein expression levels from postmortem analyses, in order to determine if DW-MRI results were correlated with tumor cell proliferation.

Materials and methods

Cell lines

Eleven low passage breast cancer cell lines (732, 812, 893, 1179, 2087, 2925, 3133, 2150, 2648, 3199 and 3171) were obtained from the University of Arizona Cancer Center (UACC) tumor cell repository. These cell lines were obtained from pleural fluids, ascites, lymph nodes, axilliary nodes or primary tumor locations, and included infiltrating ductal carcinomas, metastatic carcinomas, lobular carcinomas and adenocarcinomas. Notably, UACC-3199 and UACC-893 cell lines were derived from an infiltrating ductal carcinoma, UACC-3171 cell line from a metastatic auxiliary node carcinoma and UACC-2150 from a stage IIIB carcinoma. The status of estrogen and progesterone receptor expression was determined for each cell line using immunocytological staining while the human epidermal growth factor receptor-2 (HER2) and epidermal growth factor receptor (EGFR) status for each cell line was determined using enzyme-linked immunosorbent assay analyses.[22] Each cell line was cultured in M15 media, which consisted of Leibovitz's L-15 media buffered with 10 mmol/L HEPES, 100 U/mL penicillin, 100 μg/mL streptomycin, 0.292 mg/mL glutamine, 10 mg/L transferrin, 10^{-8} mol/L hydrocortisone, 10 mg/L insulin, 5 mg/L catalase, 5% PVP-360, 2% carboxymethylcellulose, 0.1% glutathione, DL-ornithine and orotic acid, 22 mg/L mercaptoethanol, 10.5 mol/L sodium selenite and 5% fetal bovine serum without CO_2.

Cell inoculation and tumor growth

Approximately 10^7 cells in 0.1 mL of 50% Matrigel™ (BD Biosciences, San Jose, CA, USA) in sterile saline were injected subcutaneously into the axial and inguinal mammary fat pads of female severe combined immunodeficient (SCID) mice aged four to six weeks (two mice per cell line). Mice did not receive estrogen supplementation. Tumor diameters were measured twice weekly to determine tumor volumes and doubling times (Equations (1) and (2)).

$$v = (d_{\text{short}})^2 (d_{\text{long}})^2 / 2 \quad (1)$$

$$T_{\text{d}} = (t_2 - t_1) \log(2) / \log(v_2 / v_1) \quad (2)$$

where v, v_1 and v_2 are the volumes; d_{short} and d_{long} are the short and long diameters of a tumor that is approximated to be an ellipse; T_{d} is the doubling time; and t_1 and t_2 are the time points 1 and 2, respectively.

Once the tumors of the first passage had reached approximately 400–600 mm^3 in size, one DW-MRI study was performed for each mouse. Each mouse was euthanized and non-necrotic tumor chunks approximately 2 × 2 mm in size were immediately resected and reimplanted via trochar into a set of four SCID mice. Therefore, for each cell line, the two mice from the first passage were used to create eight mice for the second passage. Two mice with UACC-3199 tumors and five mice with UACC-3171 tumors developed tumors of a viable size for this second passage, which were studied with DW-MRI using the same methodology used for studying mice of the first passage. Tumor chunks from the two mice with UACC-3199 tumors were transplanted into eight new mice, and six of these mice developed viable tumors during the third passage. Tumor chunks from two mice with UACC-3171 tumors were transplanted into eight new

mice, and two of these mice developed viable tumors during the third passage. These mice were studied with DW-MRI using the same methodology used for mice of the first and second passages. Immediately after the MRI scan, each mouse of the third passage was euthanized and tumors were flash-frozen for Western blot and immunohistochemistry analysis. All animal protocols were approved by the University of Arizona Institutional Animal Care and Use Committee.

DW-MRI

All MRI experiments were performed with a 4.7 Tesla (T) MRI scanner (Bruker Biospin Inc., Karlsuhe, Germany) equipped with an actively shielded gradient coil capable of 150 mT/m. All animals were anesthetized with 1.5% isoflurane delivered in O_2 at 1.0 L/min with temperatures continuously monitored using a rectal Luxtron® fluoroptic thermometer (Luxtron, Santa Clara, CA, USA). An external heater was used to maintain core body temperature between 36–37°C during the imaging experiments.

Contiguous axial images were obtained using a DW-MRI protocol with isotropic, radial data acquisition.[23] Diffusion-weighted images were acquired using the following parameters: repetition time (TR) = 2000 ms, echo time (TE) = 36 ms, $\Delta = 13$ ms, $\partial = 5$ ms, in-plane resolution = 200 × 200 μm, matrix size = 128 × 128, field of view (FOV) = 2.56 × 2.56 cm and slice thickness = 2.0 mm. At each slice location, images were obtained with three b values of 25, 500 or 950 s/mm^2 ($b = \gamma^2 G_d^2 \partial^2 (\Delta - \partial/3)$; G_d is the strength of the diffusion weighting gradient; γ is the gyromagnetic ratio for protons [42.58 MHz/T]; ∂ and Δ represent the duration and separation of diffusion gradients, respectively) over 20 min.

Parametric maps of the ADC were generated by fitting MRI amplitudes of each pixel to the Stejskal–Tanner equation, $S = S_0\ e^{-bADC}$, where S_0 is the signal intensity with no diffusion weighting.[24] ADC maps were processed and analyzed using programs written in Interactive Data Language (IDL; Research Systems, Boulder, CO, USA). Regions of interest corresponding to the tumor were manually prescribed on ADC maps and used to generate cumulative histograms of the ADC distributions. Cumulative histograms were produced by plotting the percent pixels greater than the ADC value versus the ADC value.

Western blot analyses

Tumor chunks from each mouse were homogenized (PowerGen 125; Fisher Scientific, Hampton, NH, USA) in cell lysis buffer containing 50 mmol/L Tris-HCl, 1% Triton X-100, 150 mmol/L NaCl and 2 mmol/L ethylenediaminetetraacetate. Total protein concentration was determined using the Bio-Rad Protein Assay Dye Reagent (Bio-Rad Laboratories, Inc., Hercules, CA, USA) with a bovine serum albumin standard. Sample aliquots of 30–40 μg of protein were denatured by heating for five minutes. Proteins were then separated by size using sodium dodecyl sulfate 10% polyacrylamide gel electrophoresis followed by transfer to polyvinylidene difluoride (PVDF) membrane using a Novex Mini-Cell Xcell II Blot Module (Invitrogen, Carlsbad, CA, USA). Blots were probed overnight at 4°C for rabbit anti-human AKT (Cell Signaling Technology [CST], Danvers, MA, USA; 1:1000), mouse monoclonal IgG phosphatase and tensin homolog (PTEN) (Cascade Bioscience, Winchester, MA, USA; 1:1000), rabbit monoclonal vascular endothelial growth factor receptor-2 (VEGFR2) (CST; 1:1000), mouse antihuman hypoxia inducible factor (HIF)-1α (Transduction Laboratories, Lexington, KY, USA; 1:250) and β-actin (Santa Cruz Biotechnologies, Santa Cruz, CA, USA; 1:10:000) in 1× Tris-buffered Saline and Tween 20. The secondary antibodies used included horseradish peroxidase (HRP)-conjugated goat anti-rabbit or goat anti-mouse immunoglobulin G (Jackson ImmunoResearch Laboratories, West Grove, PA, USA). PVDF membranes were developed using a chemiluminescence system (Amersham Pharmacia, Uppsala, Sweden).

Immunohistochemistry

In addition to the tumor chunks used for Western blot analysis, a second series of tumor chunks were fixed in neutral buffered formalin supplemented with phosphatase inhibitor cocktail 2 (Sigma-Aldrich, St Louis, MO, USA) for 24 h followed by storage in 70% ethanol. Formalin-fixed, paraffin-embedded sections sliced to approximately 3 μm thickness were deparaffinized and conditioned via antigen retrieval prior to primary antibody staining to assess HIF-1α (Transduction Laboratories; 1:50), VEGFR2 (NeoMarkers, Fremont, CA, USA; 1:10), PTEN (Cascade Bioscience; 1:100), Ki67 (Novocastra Laboratories, Buffalo Grove, IL, USA; 1:500) and hematoxylin and eosin (H&E) using a Discovery XT Automated Immunostainer (Ventana Medical Systems, Inc. [VMSI], Tucson, AZ, USA). Biotinylated universal mouse and rabbit secondary antibodies (VMSI) were applied followed by detection with strepavidin-HRP and diaminobenzidine. Deparaffinization, cell conditioning (antigen retrieval), primary antibody staining, detection and hematoxylin counterstaining were performed using validated reagents (VMSI). Following staining, slides were dehydrated through graded ethanol washes, cleared by xylene and coverslipped with Pro-Texx mounting medium (Baxter Diagnostics, Deerfield, IL, USA). Images were captured under 4X and 20X objectives using a Nikon Labophot-2 (Nikon, Inc., Melville, NY, USA) and Paxcam digital camera (MIS Inc., Villa Park, IL, USA) and PaxIt imaging software program (MIS, Villa Park, IL, USA). Images were standardized for light intensity.

Statistical analysis

Tumor growth significance was determined using repeated measures one-way analysis of variance. Molecular characterization significance was determined using a Student's t-test. Statistical significance was defined as $P \leq 0.05$.

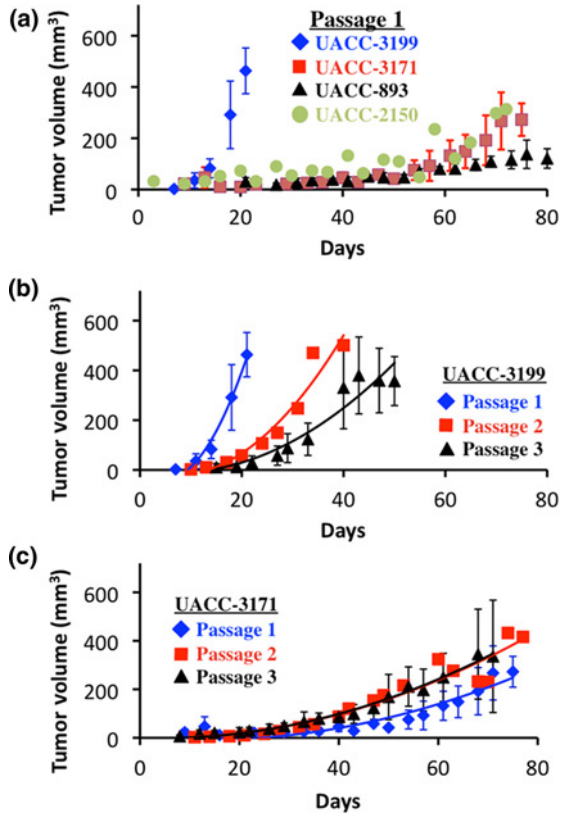

Figure 1 Tumor growth curves. (a) The first passages of the four tumor cell lines (UACC-3199, UACC-3171, UACC-893 and UACC-2150) showed moderate to rapid tumor growth. (b) Each successive passage of the UACC-3199 tumor cell line showed slower tumor growth. (c) The second and third passage of the UACC-3171 tumor cell line showed slower tumor growth than the first passage. (A color version of this figure is available in the online journal)

Results

In vivo tumor growth of breast cancer cell lines exhibits different growth rates

Of the 11 breast cancer cell lines tested, only four cell lines (UACC-2150, UACC-3199, UACC-3171 and UACC-893) grew to a minimum tumor volume of 350 mm^3 within 120 d during passage 1 (Figure 1a). Notably, these four cell lines had the highest aerobic glycolytic activity among all cell lines tested.[22] The UACC-3199 cell line showed a fast growth rate of 22.1 mm^3/d and a doubling time of 3.2 d, while the other three cell lines showed a moderate growth rate of 2.3–4.9 mm^3/d and doubling times of 16–48 d (Table 1). The remaining seven cell lines grew to less than 100 mm^3 within 120 d, and therefore were not passaged. Of the four cell lines that were initially passaged, only UACC-3199 and UACC-3171 grew to a minimum tumor volume of 350 mm^3 and were able to be serially reimplanted in mice for three passages (Figures 1b and c, respectively). The UACC-2150 and UACC-893 cell lines only grew to less than 100 mm^3 during the second passage. A delay in tumor growth rate and an increase in doubling time was observed in UACC-3199 tumor xenografts from passage 1 to passage 3 but remained consistent in UACC-3171 tumor xenografts throughout three passages.

DW-MRI of UACC-3199 and UACC-3171 tumor xenografts

The DW-MRI studies showed that a greater average ADC was observed in UACC-3171 tumor xenografts compared with UACC-3199 tumor xenografts (Figure 2a). However, the average ADC value of a tumor fails to reflect the distribution of pixel values, which may also have diagnostic value (Figure 2b). Therefore, the ADC throughout the tumor was also evaluated using cumulative histograms (Figures 2c and d). In studies of all cell lines and all passages, the distribution of pixel-wise ADC values reflected a normal distribution, which validated that constructing cumulative histograms was appropriate for this evaluation. An increasing ADC distribution was observed through the passages of UACC-3199 tumors, which also correlated with the decreasing growth rate during each passage. The ADC distribution of UACC-3171 tumors increased between passages 1 and 2 and remained steady thereafter (Figure 2d). This matched the correlation between the mean ADC and relative growth rates observed with each passage (Figure 3). The ADC distribution was lower for UACC-3199 tumor xenografts relative to UACC-3171 tumor xenografts for each passage, which also correlated with the faster growth rates of UACC-3199 tumor xenografts relative to UACC-3171 tumor xenografts.

Expression of signaling proteins in the AKT/VEGF pathways

Western blots were performed to quantify the expression of AKT, PTEN, VEGFR2 and HIF-1α in the UACC-3199 and UACC-3171 tumor tissue homogenates after the third passage in mice (Figure 4a). Expression levels were normalized to the expression of β-actin to account for variability in total protein between tissues and thus was used as an internal control. Both cell lines showed high expression of AKT, PTEN and VEGFR2, and relatively lower expression of HIF-1α (Figure 4b). The UACC-3199 cells showed

Table 1 Growth rate and doubling time of tumor xenografts

	Growth rate (mm^3/d)			Doubling time (d)			Number		
Cell line	Pass 1	Pass 2	Pass 3	Pass 1	Pass 2	Pass 3	Pass 1	Pass 2	Pass 3
UACC-893	2.3			48.2			2	0	0
UACC-2150	4.4			17.7			2	0	0
UACC-3199	22.1	12.5	4.8	3.2	7.6	13.5	2	2	6
UACC-3171	4.9	3.8	3.9	16.4	28.1	18.4	2	5	2

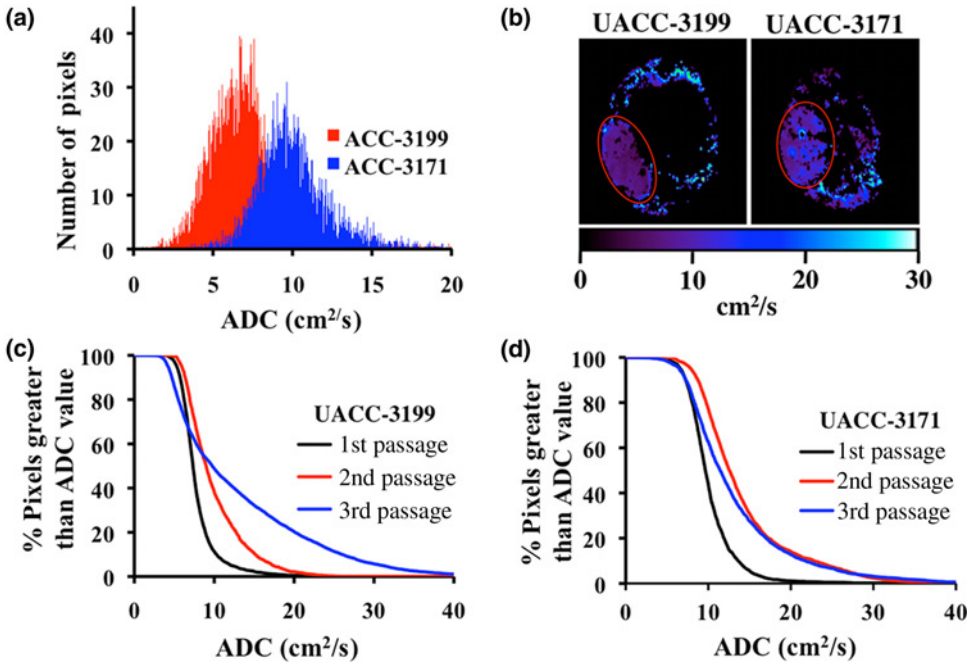

Figure 2 (a) The histograms of ADC values determined from (b) pixels in the regions of interest (circles) in the representative ADC parametric maps showed a lower average ADC for the faster-growing UACC-3199 tumor xenograft relative to the UACC-3171 xenograft. (c) Cumulative histograms of ADC values of the UACC-3199 tumor xenograft showed distributions with increasing ADC values for each successive passage. (d) Cumulative histograms of ADC values of the UACC-3171 tumor xenograft showed distributions with higher ADC values for the second and third passage relative to the first passage. Data represent a whole tumor of a single representative mouse. ADC, apparent diffusion coefficient. (A color version of this figure is available in the online journal)

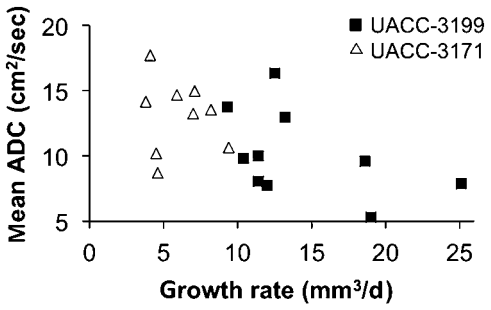

Figure 3 The mean ADC value showed a weak correlation with growth rate for each tumor. ADC, apparent diffusion coefficient

significantly higher expression of VEGFR2, PTEN and HIF-1α compared with UACC-3171 cells. However, the expression of AKT showed no statistically significant differences between the UACC-3199 and UACC-3171 xenografts. Qualitative *in vitro* analyses verified that both of these cell lines were ER-, PR- and HER-2 negative, and the UACC-3199 cell line was EGFR-positive while the UACC-3171 cell line was EGFR-negative.[22]

Immunohistochemical evaluation of signaling proteins

Immunohistochemistry was performed to evaluate the level and spatial distribution of VEGFR2 and HIF-1α expressions. VEGFR2 was strongly detected in both UACC-3199 and UACC-3171 tumor xenografts with good spatial homogeneity throughout the tissue sample. VEGFR2 expression was observed to be higher in UACC-3199 tumor xenograft (100% 2+ cytoplasmic/10% 2+ nuclear) than the UACC-3171 xenograft (80% 1+ cytoplasmic/20% 2+ nuclear), which was consistent with the Western blot analyses. The immunohistochemical detection of HIF-1α in both UACC-3199 (30% 2+ nuclear) and UACC-3171 (5% 1+ nuclear) tumor xenografts demonstrated weaker and more spatially heterogeneous staining relative to VEGFR2, which was also consistent with the Western blot analyses. A molecular biomarker of cell proliferation, Ki67, was present in 85% of the UACC-3199 cell line and in 80% of the viable tumor portion of the UACC-3171 cell line. H&E staining demonstrated 100% viable cells in the UACC-3199 cell line compared with 20% in the UACC-3171 cell line. Staining for PTEN showed an insignificant expression throughout the tumor but predominant staining in the vascularized area of the tumors.

Discussion

Historically, human breast tumors are one of the most difficult tumor type to grow as xenotransplants, with take rates of about 27% compared with take rates of 50–70% that are seen in colorectal, ovarian, melanoma and lung tumors.[25–28] In the current study, only two of 11 low passage lines were able to be serially transplanted for more than one passage in SCID mice, which agrees with previously published studies. Some human breast tumors require estrogen supplements to grow as xenotransplants, which may partly explain the low take rate of breast cancer when estrogen supplements are not used. Ten of the 11 cell lines used in this study were ER−, so this study did not use estrogen supplementation when developing xenotransplants. The UACC-2648 cell line was ER+,

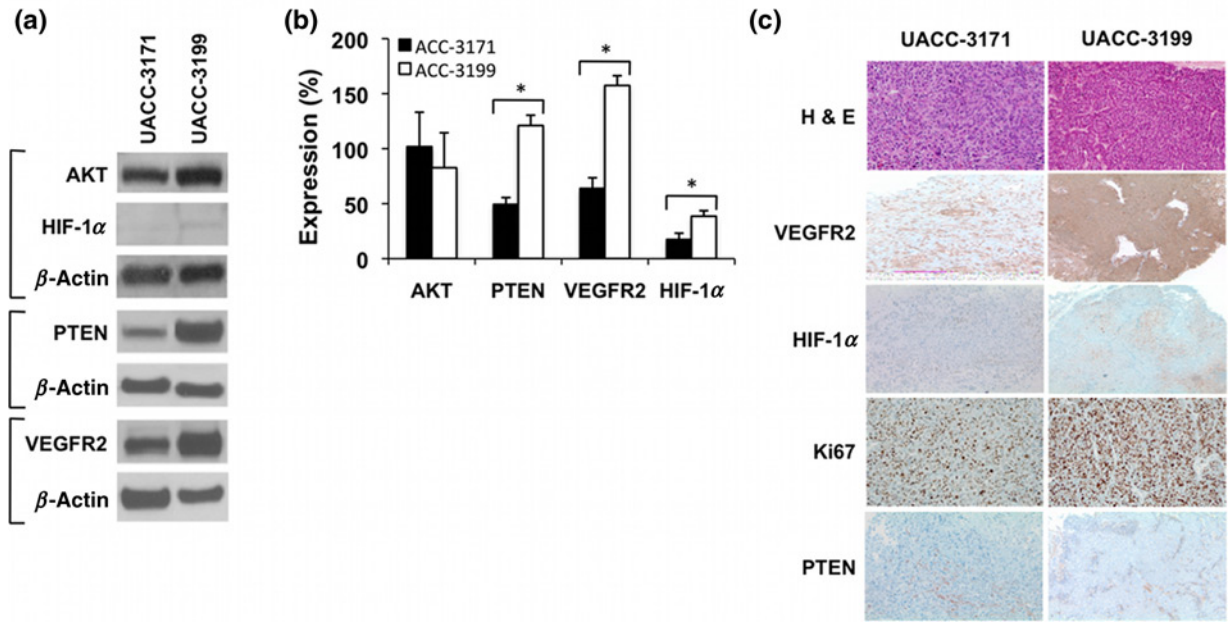

Figure 4 (a) The expressions of AKT, PTEN, VEGFR2 and HIF-1α in UACC-3199 and UACC-3171 cell lines were analyzed using Western blots. Each expression was normalized to the expression of β-actin. (b) The faster-growing tumor cell line, UACC-3199, showed greater PTEN, VEGFR2 and HIF-1α expressions ($^*P < 0.05$) relative to the UACC-3171 cell line, while AKT expression was not significantly different between cell lines. (c) Immunostaining showed higher VEGFR2, HIF-1α and Ki67 expressions in UACC-3199 tumors relative to UACC-3171 tumors, and also showed greater hematoxylin and eosin staining in the UACC-3199 tumors. PTEN staining was very low in both tumor types. Magnification, $\times$20. (A color version of this figure is available in the online journal)

which may explain the lack of tumor growth for this particular cell line without estrogen supplementation. Notably, the UACC-3199 and UACC-3171 cell lines that were passaged more than once were triple-negative (ER/PR/HER-2), whereas the UACC-2150 and UACC-893 express HER-2/neu and were only able to be passaged once.[22]

The slower tumor growth rates and longer doubling times of the UACC-3199 and UACC-3171 tumor xenografts during the second and third passages were in contrast to previous studies.[29–31] Yet, heterotransplants have varied growth rates between passages due to changes in proliferative activity of the tumor cell, cell loss including loss of a stem cell population and other cell fractions that promote growth, and lower take rate of surgical tissue following transplantation.[26,32] Tissue handling including transit time from removal of the surgical tissue to reimplantation may also contribute to variability in growth rate, although we took care to minimize transit time following tumor excision.[26] Our results may reflect a combination of these factors. Despite this variability of lag times, our results showed that the UACC-3199 and UACC-3171 cell lines could form reproducible xenograft tumor models for our subsequent analyses.

All DW-MRI results showed that a shift of the distribution to a lower average ADC value was correlated with faster tumor growth rates and shorter doubling times. The normal distributions of the ADC values suggest that the tumor growth was uniform throughout the tumor. This correlation is particularly exemplified by the lower ADC distribution for the first passage of the fast-growing UACC-3199 and UACC-3171 tumor xenografts, relative to the higher ADC distributions of the slower-growing second and third passages of these cell lines. This correlation was also observed for the faster-growing UACC-3199 tumor xenografts relative to the UACC-3171 xenografts. As shown by other DW-MRI studies, a shift of the distribution to a lower average ADC value generally indicates a lower percentage of extracellular space in the tumor microenvironment and a higher cell density in the tumor tissue.[14–16] Therefore, these correlations showed that DW-MRI can be used to verify lower extracellular space and higher cell densities caused by faster growth rates and shorter doubling times, so that DW-MRI can provide good utility for assessing new tumor models.

These qualitative assessments of the shifts of distributions of ADC values were useful for initially establishing new cancer models. The intrinsic limitations to qualitative assessment of these cumulative histograms include reliability and validity of the results as well as wider interpretation to other tumor mouse models. However, future studies that are designed for a more rigorous quantitative analysis of these ADC distributions can be initiated. For example, a two-sample Kolmogorov–Smirnov test can be used to determine if two distributions are statistically distinct based on the locations and shapes of the empirical cumulative distribution functions.[33] Similarly, a *K*-sample Anderson–Darling test can be used to determine whether two distributions are distinct.[34] As another example, the Shapiro–Wilk test can reveal if results represent a normally distributed population, which can be used to determine if each distribution indicates that tumor growth was uniform throughout the tumor.[35] However, a greater number of mice per model is needed to interpret these quantitative comparisons of ADC distributions or cumulative distributions and therefore we limited our initial study to qualitative comparisons.

The Ki67 stainings indicated similar proliferation in the viable regions of the UACC-3199 and UACC-3171 tumor xenografts. Yet, the H&E stainings indicated that only 20% UACC-3171 xenograft tissue was viable, compared with 100% viability for the UACC-3199 xenograft. Therefore, the proliferation in the total tumor was higher for the entire UACC-3199 xenograft tumor relative to the UACC-3171 xenograft. This difference in tumor cell proliferation correlated with the shift of the distribution to a lower average ADC value, increased tumor growth rates and shorter doubling times of the UACC-3199 xenograft.

The UACC-3199 tumor xenografts had higher expression of HIF-1α and VEGFR2 compared with UACC-3171 xenografts, which was correlated with a shift of the distribution to a lower average ADC value, increased tumor growth rates and shorter doubling times in the UACC-3199 xenografts. This was expected, because up-regulation of HIF-1α elicits a multiphasic response that includes increased aerobic glycolysis, which in turn promotes tumor cell proliferation.[36,37] In addition, HIF-1α also elicits angiogenesis by increasing expression of VEGFR2 and other growth factors. VEGFR2 leads to neovascularization and increased vascular permeability in tumors, which provides nutrients for tumor growth resulting in increased tumor cell proliferation.[38] Furthermore, VEGFR2 expression is promoted by additional signaling pathways which may justify the greater expression of VEGFR2 relative to HIF-1α in these studies.[39] Clinically, HIF-1α expression is associated with a worse prognosis across all breast cancer subtypes.[40] VEGFR2 expression is more specifically associated with the triple-negative breast cancer phenotype, and is also associated with a worse prognosis.[41] Interestingly, the UACC 3199 cell line is EGFR+, HIF-1α+ and VEGFR2+ which are all hallmarks of aggressive triple-negative tumors. Therefore, the UACC 3199 represents a valuable model to study this tumor type *in vivo*.

The UACC-3199 tumor xenografts showed higher expression of PTEN compared with UACC-3171 xenografts. PTEN selectively dephosphorylates phosphoinositol trisphosphate (PIP_3), which regulates the cell cycle and acts as a tumor suppressor by reducing cell proliferation.[42] PTEN also negatively regulates the activation of AKT, which promotes tumor cell survival in combination with the phosphoinositide 3-kinase/mammalian target of rapamycin pathway.[43] Yet the AKT expression levels of the UACC-3199 and UACC-3171 tumor xenografts were not statistically different from each other, suggesting that the increased expression of PTEN in the UACC-3199 xenograft did not negatively regulate AKT in this tumor model, and therefore did not reduce cell proliferation. Tumor cells often express inactive PTEN that fails to regulate tumor growth, which may further justify these results.[44] Therefore, PTEN expression and tumor cell proliferation are not necessarily correlated, which justifies a higher PTEN level and a shift of the distribution to a lower average ADC value in the UACC-3199 tumor xenograft relative to the UACC-3177 xenograft. The observation that PTEN in the more viable UACC-3199 tumor, and that PTEN staining was only predominant in the vascularized area of the tumors, may indicate that PTEN promotes anti-apoptosis through an AKT-independent mechanism in this model.[45] More generally, cell signaling and regulation depend on a complex network of pathways, so that the expression levels of some proteins such as VEGFR2 and HIF-1α may correlate with tumor cell proliferation, and yet other proteins such as PTEN may not necessarily correlate with tumor cell proliferation. This result demonstrates that the distribution of ADC values from DW-MRI may be a more functional evaluation of tumor cell proliferation.

In summary, we have shown that the distribution of ADC values from DW-MRI studies are correlated with tumor growth rates and expression of signaling proteins that promote cell proliferation. DW-MRI is unlikely to replace tumor size measurements as the 'gold standard' for assessing tumor proliferation, due to the high cost and moderate expertise required for DW-MRI studies. Yet, this study has established that DW-MRI can provide additional diagnostic information about new preclinical models of human cancers that can augment tumor growth rate measurements. In addition, this study further establishes that the UACC-3199 and UACC-3171 cell lines can be used to develop xenograft tumor models of triple-negative breast cancer.

Author contributions: All authors participated in the design, interpretation of the studies, analysis of the data and review of the manuscript. RMS conducted the DW-MRI experiments; RMS, RJG and MDP analyzed and interpreted the DW-MRI results; RMS, KB, AFB and EJM conducted the studies that assessed signaling proteins; and RMS and MDP wrote the manuscript.

ACKNOWLEDGEMENTS

This work was supported by the Arizona Cancer Center and the National Cancer Institute under grants P50 CA95060, PO1 CA017094, R01 CA125627, R01 CA077575, P30 CA023074 and U54 CA90821. The authors thank Dr Jean Phillipe Galons and Ms Christy Howison for assistance with MRI studies. The authors also thank the Experimental Mouse, Tissue Acquisition and Cellular/Molecular Analysis and Biometry Core Shared Services of the Arizona Cancer Center for their outstanding contributions to this multidisciplinary research project.

REFERENCES

1 Cariati M, Marlow R, Dontu G. Xenoplantation of breast cancers. *Methods Mol Biol* 2011;**731**:471–82
2 Schumacher U, Brooks SA. Xenograft models in immunodeficient animals: II. The use of SCID mice in metastasis research: breast and colon cancer models of metastasis. *Methods Mol Med* 2001;**58**:215–22
3 Gillies RJ, Gatenby RA. Hypoxia and adaptive landscapes in the evolution of carcinogenesis. *Cancer Met Rev* 2007;**26**:311–17
4 Vargo-Gogola T, Rosen JM. Modelling breast cancer: one size does not fit all. *Nature Rev Cancer* 2007;**7**:659–72
5 Naf D, Krupke DM, Sundberg JP, Eppig JT, Bult CJ. The mouse tumor biology database: a public resource for cancer genetics and pathology of the mouse. *Cancer Res* 2002;**62**:1235–40
6 Krupke DM, Naf D, Vincent MJ, Allio T, Mikaelian I, Sundberg JP, Bult CJ, Eppig JT. The mouse tumor biology database: integrated access to mouse biology data. *Exp Lung Res* 2005;**31**:259–70

7 Tomayko MM, Reynolds CP. Determination of subcutaneous tumor size in athymic (nude) mice. *Cancer Chemother Pharmacol* 1989;**24**:148–54
8 Schlom J, Wunderlick DR, Teramoto Y. Generation of human monoclonal antibodies reactive with human mammary carcinoma cells. *Proc Natl Acad Sci USA* 1980;**77**:6841–5
9 Tan PH, Bay BH, Yip G, Selvarajan S, Tan P, Wu J, Lee CH, Li KB. Immunohistochemical detection of Ki67 in breast cancer correlates with transcriptional regulation of genes related to apoptosis and cell death. *Modern Pathol* 2005;**18**:374–81
10 Bammer R. Basic principles of diffusion-weighted imaging. *Eur J Radiol* 2003;**45**:169–84
11 Padhani AR, Liu G, Koh DM, Chenevert TL, Thoeny HC, Takahara T, Dzik-Jurasz A, Ross BD, Van Cauteren M, Collins D, Hammoud DA, Rustin GJ, Taouli B, Choyke PL. Diffusion-weighted magnetic resonance imaging as a cancer biomarker: consensus and recommendations. *Neoplasia* 2009;**11**:102–25
12 Gibbs P, Liney GP, Pickles MD, Zelhof B, Rodrigues G, Turnbull LW. Correlation of ADC and T2 measurements with cell density in prostate cancer at 3.0 Tesla. *Invest Radiol* 2009;**44**:572–6
13 Schnapauff D, Zeile M, Niederhagen MB, Fleige B, Tunn PU, Hamm B, Dudeck O. Diffusion-weighted echo-planar magnetic resonance imaging for the assessment of tumor cellularity in patients with soft-tissue sarcomas. *J Magn Reson Imaging* 2009;**29**:1355–9
14 Wang XZ, Wang B, Gao ZQ, Liu JG, Liu ZQ, Niu QL, Sun ZK, Yuan YX. Diffusion-weighted imaging of prostate cancer: correlation between apparent diffusion coefficient values and tumor proliferation. *J Magn Reson Imaging* 2009;**29**:1360–6
15 Gillies RJ, Raghunand N, Karczmar GS, Bhujwalla ZM. MRI of the tumor microenvironment. *J Magn Reson Imaging* 2002;**16**:430–50
16 Kim H, Morgan DE, Zeng H, Grizzle WE, Warram JM, Stockard CR, Wang D, Zinn KR. Breast tumor xenografts: diffusion-weighted MR imaging to assess early therapy with novel apoptosis-inducing anti-DR5 antibody. *Radiology* 2008;**248**:844–51
17 Vossen JA, Buijs M, Geschwind JFH, Liap E, Ventura VP, Lee KH, Bluemke DA, Kamel IR. Diffusion-weighted and Gd-EOB-DTPA contrast-enhanced magnetic resonance imaging for characterization of tumor necrosis in an animal model. *J Comput Assist Tomogr* 2009;**33**:626–30
18 Galons JP, Morse DL, Jennings DR, Gillies RJ. Diffusion-weighted MRI and response to anti-cancer therapies. *Isreal J Chem* 2003;**43**:91–101
19 Theilmann RJ, Borders R, Trouard TP, Xia G, Outwater E, Ranger-Moore J, Gillies RJ, Stopeck A. Changes in water mobility measured by diffusion MRI predict response of metastatic breast cancer to chemotherapy. *Neoplasia* 2004;**6**:831–7
20 Jordan BF, Runquist M, Raghunand N, Baker A, Williams R, Kirkpatrick L, Powis G, Gillies RJ. Dynamic contrast-enhanced and diffusion MRI show rapid and dramatic changes in tumor microenvironment in response to inhibition of HIF-1alpha using PX-478. *Neoplasia* 2005;**7**:475–85
21 Morse DL, Galons JP, Payne CM, Jennings DL, Day S, Xia G, Gillies RJ. MRI-measured water mobility increases in response to chemotherapy via multiple cell-death mechanisms. *NMR Biomed* 2007;**20**:602–14
22 Robey IF, Stephen RM, Brown KS, Baggett BK, Gatenby RA, Gillies RJ. Regulation of the Warburg effect in early-passage breast cancer cells. *Neoplasia* 2008;**10**:745–56
23 Trouard TP, Theilmann RJ, Altbach MI, Gmitro AF. High-resolution diffusion imaging with DIFRAD-FSE (diffusion-weighted radial acquisition of data with fast spin-echo) MRI. *Magn Reson Med* 1999;**42**:11–8
24 Stejskal EO, Tanner JE. Spin diffusion measurements: spin echoes in the presence of a time-dependent field gradient. *J Chem Phys* 1965;**42**:288–92
25 Fogh J, Tiso J, Orfeo T, Sharkey FE, Daniels WP, Fogh JM. Thirty-four lines of six human tumor categories established in nude mice. *J Natl Cancer Inst* 1980;**64**:745–51
26 Mattern J, Bak M, Hahn EW, Volm M. Human tumor xenografts as model for drug testing. *Cancer Met Rev* 1988;**7**:263–84
27 Li Z, Huang X, Li J, Ke Y, Yang L, Wang Y, Yao L, Lu Y. Human breast carcinoma xenografts in nude mice. *Chin Med J (Engl)* 2002;**115**:222–6
28 Shimosato Y, Kameya T, Nagai K, Hirohashi S, Koide T, Hayashi H, Nomura T. Transplantation of human tumors in nude mice. *J Natl Cancer Inst* 1976;**56**:1251–60
29 Houghton JA, Taylor DM. Growth characteristics of human colorectal tumours during serial passage in immune-deprived mice. *Br J Cancer* 1978;**37**:213–23
30 Mattern J, Wayss K, Haag D, Toomes H, Volm M. Different growth rates of lung tumours in man and their xenografts in nude mice. *Eur J Cancer* 1980;**16**:289–91
31 Corbett T, Griswold D, Roberts B, Schnabel F. Cytotoxic adjuvant therapy and the experimental model. In: Stoll BA, ed. *New Aspects of Breast Cancer. Systemic Therapy in Breast Cancer*. Vol. 4. London: William Heinemann Medical Books, LTD, 1981
32 Clarke R. Issues in experimental design and endpoint analysis in the study of experimental cytotoxic agents *in vivo* in breast cancer and other models. *Breast Cancer Res Treat* 1997;**46**:255–78
33 Fasano G, Franceschini A. A multidimensional version of the Kolmogorov-Smirnov test. *R Astron Soc* 1987;**225**:155–70
34 Anderson TW, Darling DA. Asymptomatic theory of certain 'goodness-of-fit' criteria based on stochastic processes. *Ann Math Stat* 1952;**23**:193–212
35 Shapiro SS, Wilk MB. An analysis of variance test for normality (complete samples). *Biometrika* 1965;**52**:591–611
36 Greijer AE, van der Groep P, Kemming D, Shvarts A, Smezna GL, Meijer GA, van de Wiel MA, Belien JA, van Diest PJ, van der Wall E. Up-regulation of gene expression of by hypoxia is mediated predominantly by hypoxia-inducible factor 1 (HIF-1). *J Pathol* 2005;**206**:291–304
37 Gatenby RA, Gillies RJ. Glycolysis in cancer: a potential target for therapy. *Int J Biochem Cell Biol* 2007;**39**:1358–66
38 Liang Y, Brekken RA, Hyder SM. Vascular endothelial growth factor induces proliferation of breast cancer cells and inhibits the anti-proliferative activity of anti-hormones. *Endocr Relat Cancer* 2006;**13**:905–19
39 Holmes K, Roberts OL, Thomas AM, Cross MJ. Vascular endothelial growth factor receptor-2: structure, function, intracellular signalling and therapeutic inhibition. *Cellular Signalling* 2007;**19**:2003–12
40 Trastour C, Benizri E, Ettore F, Ramaioli A, Chamorey E, Pouysségur J, Berra E. HIF-1alpha and CA IX staining in invasive breast carcinomas: prognosis and treatment outcome. *Int J Cancer* 2007;**120**:1451–8
41 Rydén L, Jirström K, Haglund M, Stål O, Fernö M. Epidermal growth factor receptor and vascular endothelial growth factor receptor 2 are specific biomarkers in triple-negative breast cancer. Results from a controlled randomized trial with long-term follow-up. *Breast Cancer Res Treat* 2010;**120**:491–8
42 Steck PA, Pershouse MA, Jasser SA, Yung WK, Lin H, Ligon AH, Langford LA, Baumgard ML, Hattier T, Davis T, Frye C, Hu R, Swedlund B, Teng DH, Tavtigian SV. Identification of a candidate tumour suppressor gene, MMAC1, at chromosome 10q23.3 that is mutated in multiple advanced cancers. *Nat Genet* 1997;**15**:356–62
43 Vivanco I, Sawyers CL. The phosphatidylinositol 3-kinase AKT pathway in human cancer. *Nat Rev Cancer* 2002;**2**:489–501
44 Li J, Yen C, Liaw D, Podsypanina K, Bose S, Wang SI, Puc J, Miliaresis C, Rodgers L, McCombie R, Bigner SH, Giovanella BC, Ittmann M, Tycko B, Hibshoosh H, Wigler MH, Parsons R. PTEN, a putative protein tyrosine phosphatase gene mutated in human brain, breast, and prostate cancer. *Science* 1997;**275**:1943–7
45 Blanco-Aparicio C, Renner O, Leal JFM, Carnero A. PTEN, more than the AKT pathway. *Carcinogenesis* 2007;**28**:1379–86

(Received September 30, 2011, Accepted August 12, 2012)